

## A WEIGHTED COHERENCE ESTIMATOR FOR COHERENT CHANGE DETECTION IN SYNTHETIC APERTURE RADAR IMAGES

Mengmeng Wang<sup>1</sup>, Guoman Huang<sup>2</sup>, Jixian Zhang<sup>3</sup>, Fenfen Hua<sup>4</sup>, Lijun Lu<sup>2</sup> \*

<sup>1</sup> School of Environment and Spatial Informatics, China Univ. of Mining and Technology, 1 Daxue Road, Xuzhou, China - wangmemie@cumt.edu.cn

<sup>2</sup> Chinese Academy of Surveying and Mapping, Beijing, China - huang.guoman@casm.ac.cn, lulj@casm.ac.cn

<sup>3</sup> National Quality Inspection and Testing Center for Surveying and Mapping Products, Beijing, China - zhangjx@casm.ac.cn,

<sup>4</sup> Jiangsu Normal Univ., Xuzhou, China - Huaufenfen\_hff@163.com

**KEY WORDS:** Coherence Estimator, Coherent Change Detection, Maximum Likelihood, Synthetic Aperture Radar, Weighted Estimator.

### ABSTRACT:

Synthetic aperture radar (SAR) coherent change detection (CCD) often utilizes the degree of coherence to detect changes that have occurred between two data collections. Although having shown some performances in change detection, many existing coherence estimators are still relatively limited because the change areas do not stand out well from all decorrelation areas due to the low cluster-to-noise ratio (CNR) and volume scattering. Moreover, many estimators require the equal-variance assumption between two SAR images of the same scene. However, the assumption is less likely to be met in regions of significant differences in intensity, such as the change areas. To address these problems, we proposed an improved coherence estimator that introduces the parameters about the true-variance ratio as the weights. Since these parameters are closely related to the ratio-change statistic in intensity-based change detection algorithms, their introduction frees the estimator from the need for the equal-variance assumption and enables detection results to largely combine the advantages of intensity-based and CCD methods. Experiments on simulated and real SAR image pairs demonstrate the effectiveness of the proposed estimator in highlighting the change, obviously improving the contrast between the change and the background.

### 1. INTRODUCTION

Synthetic aperture radar (SAR) has been an important modality in remote sensing because of its capability to obtain high-resolution images with weather and lighting conditions independent. As one of the popular applications, SAR change detection utilizes two SAR images of the same scene taken at different times to detect changes that have occurred between the two acquisition dates (Massonnet, Feigl, 1998). There are generally two forms of traditional SAR change detection: coherent and incoherent change detection. Incoherent change detection uses SAR intensity images to identify large-scale changes, whereas coherent change detection (CCD) utilizes SAR phase and intensity to estimate the coherence to detect small-scale changes (Cha et al., 2015).

As a measurement of the change, the coherence statistics often provide low value in change areas. However, low coherence or decorrelation can be caused by many sources, such as the baseline or geometric decorrelation, thermal or system noise, volume decorrelation, and temporal terrain decorrelation (Hanssen, 2001). For a given pair of spatial-registered SAR images, the sources of decorrelation to be considered mainly contain temporal decorrelation, volume decorrelation, and low clutter-to-noise ratio (CNR) decorrelation. Among them, temporal decorrelation is caused by physical changes in the terrain. Obviously, changes that have occurred between two data collections, the interest of change detection, can lead to this temporal decorrelation. Volume scattering due to the penetration of the radar wave in the scattering medium often happens in vegetation terrain where vegetation growth can also

inevitably cause temporal decorrelation, bringing about disturbances for most change detection tasks. The last low-CNR decorrelation can occur for many features in the SAR scene, such as shadow areas, hard-packed roads, and smooth surfaces (Wahl et al., 2016). As we know CCD aims at detecting changes between two SAR images, therefore, the capability of coherence estimators in distinguishing change areas from all decorrelation areas has an important influence on the accuracy of the detection results.

Now many coherence estimators have been proposed. In the beginning, the coherence statistic is often used for terrain height measures for interferometric SAR images (Rodriquez, Martin, 1992). In 1996, the coherence estimator was first introduced into change detection to detect anthropogenic temporal changes (Jakowatz et al., 1996). In order to overcome low coherence measurements caused by low CNR in SAR images, some workers suggested masking the potential low-CNR areas using the CNR information from SAR images (Yocky, Johnson, 1998). Other authors proposed some log-likelihood change statistics (Preiss et al., 2006; Wahl et al., 2016; Zhao et al., 2017). In addition, some changes methods combining coherent and incoherent algorithms have been presented for SAR change detection (Cha et al., 2015; Yang et al., 2015). Among them, coherent approaches similarly utilize the above-mentioned coherent estimators. Although achieving some performance, these estimators are still limited because the change areas do not stand out well from all decorrelation areas due to low CNR and volume scattering. In particular, the boundaries between change and no-change regions are fuzzy and difficult to determine, unfavorable for obtaining fine change maps.

\* Corresponding author

Besides, many existing coherence estimators require the equal-variance assumption should be met between two SAR images. It has been investigated that the variance of a given pixel in a SAR image is determined by the scattering amplitudes and is closely related to the average intensity (Oliver and Quegan, 2004). However, there are often significant intensity differences in change areas, which makes the equal-variance assumption less likely to be met in these areas. Consequently, the change information may not be nicely highlighted using these estimators.

In this paper, a novel weighted estimator has been proposed to address the above problems. The estimator is derived based on the statistical characteristics of SAR images by using the ML principle. As the weighted parameters are closely related to the ratio change statistic used in intensity-based noncoherent algorithms, its introduction into the derivation makes the estimator largely combine the advantages of coherent and noncoherent algorithms. Experiments on simulated and real SAR image pairs show the effectiveness of the weighted estimator in highlighting changes, significantly improving the contrast between the change and the background.

The main contribution of this paper is the introduction of the ratio change statistic into the estimation of the coherence estimator. The organization for the remainder of this paper is as follows. Section 2 presents some common coherence estimators and their limitations. Section 3 derives the new coherence estimator. Section 4 evaluates the performance of the proposed estimator on simulated and real SAR image pairs. Section 5 concludes this paper.

## 2. COMMON COHERENT ESTIMATORS

As a change metric of CCD, the coherence  $\gamma$  is often estimated using a classical coherence estimator (Rodriquez and Martin, 1992):

$$\hat{\gamma}_c = \frac{\left| \sum_{k=1}^N f_k^* g_k \right|}{\sqrt{\sum_{k=1}^N f_k^* f_k \sum_{k=1}^N g_k^* g_k}}, \quad (1)$$

where  $\mathbf{f}, \mathbf{g} = N$ -sample, zero-mean Gaussian random vectors  
 $f_k, g_k = k^{\text{th}}$  observation of vectors  $\mathbf{f}$  and  $\mathbf{g}$   
 $*$  = complex conjugate operation  
 $\wedge$  = estimator of the parameter

The estimator  $\hat{\gamma}_c$  and its modifications (Guarnieri and Prati, 1997) are mainly used in interferometric SAR tasks for terrain height generation. As a measure of the similarity degree,  $\hat{\gamma}_c$  will provide low coherence values in low-similarity regions such as change, low-CNR, and many vegetation regions, leading to the mixture of all decorrelation regions and the failure of distinguishing change areas. To address this problem, a complex reflectivity change model was introduced into CCD and expressed as (Jakowatz et al., 1996):

$$\hat{\gamma}_m = \frac{2 \left| \sum_{k=1}^N f_k^* g_k \right|}{\sum_{k=1}^N f_k^* f_k + \sum_{k=1}^N g_k^* g_k}. \quad (2)$$

The estimator  $\hat{\gamma}_m$  has been demonstrated better than  $\hat{\gamma}_c$ , having the ability to differentiate the changes from the background. As we know, change regions generally have low-coherence values

as well as obvious intensity differences. However, in low-CNR regions, such as hard-packed roads and smooth water surfaces, or many vegetation areas with the property of volume scattering, if not changed, the intensity of two SAR images would not significantly differ from each other. Several methods have been proposed to overcome low-CNR decorrelation, typically the complex reflectance change detection (CRCD) metric (Wahl et al.):

$$\hat{\gamma}_\alpha = \frac{2 \left| \sum_{k=1}^N f_k^* g_k \right|}{\sum_{k=1}^N f_k^* f_k + \sum_{k=1}^N g_k^* g_k - N\sigma_{nf}^2 - N\sigma_{ng}^2}, \quad (3)$$

where  $\sigma_{nf}^2, \sigma_{ng}^2 =$  variances of the additive system thermal noise of vectors  $\mathbf{f}$  and  $\mathbf{g}$

Although these estimators have achieved some performance in change detection, it is still a difficult task for them to identify change areas because of the decorrelation due to low CNR and volume scattering. Besides, most of them require equal variances of two SAR images. However, the equal-variance assumption is unlikely to be met due to the presence of scene disturbances during the two collections as well as antenna-pointing errors arising in the data collection and radiometric miscalibration in the image formation (Preiss et al., 2006), especially in change areas with significant intensity differences. Therefore, the effective identification of changes and the assumption of equal variance are two key problems to be solved for an optimal coherence estimator.

## 3. METHODOLOGY

### 3.1 Statistical Properties of SAR Image Pair

The SAR data, known as the complex image, is consisted of the observed in-phase and quadrature components,  $z_1 = A \cos \phi$  and  $z_2 = A \sin \phi$  where  $A$  is the amplitude and  $\phi$  is the phase. Two components will be independent identically distributed zero-mean Gaussian random variables whose joint probability density function (PDF) can be expressed as:

$$p(z_1, z_2) = \frac{1}{\pi\sigma^2} \exp\left(-\frac{z_1^2 + z_2^2}{\sigma^2}\right), \quad (4)$$

where  $\sigma^2 =$  average intensity

Given two spatial-registered SAR images, one can form a joint data vector  $\mathbf{X} = [\mathbf{f}, \mathbf{g}]^T$  from the corresponding  $N$ -pixel local neighborhoods. And the PDF of the vector  $\mathbf{X}$  is given by:

$$p(\mathbf{X} | \gamma, \varphi) = \frac{1}{\pi^{2N} |\mathbf{Q}|^N} \exp\left(-\sum_{k=1}^N \mathbf{X}_k^H \mathbf{Q}^{-1} \mathbf{X}_k\right), \quad (5)$$

where  $\mathbf{H} =$  complex conjugate transpose operation

$$\mathbf{Q} = E(\mathbf{X}\mathbf{X}^H) = \begin{bmatrix} \sigma_f^2 & \gamma\sigma_f\sigma_g e^{j\varphi} \\ \gamma\sigma_f\sigma_g e^{-j\varphi} & \sigma_g^2 \end{bmatrix}$$

where  $\sigma_f^2 = E(\mathbf{f}\mathbf{f}^*)$

$\sigma_g^2 = E(\mathbf{g}\mathbf{g}^*)$

$\gamma =$  magnitude of complex coherence

$\varphi =$  constant phase difference

$|\mathbf{Q}|$  = determinant of  $\mathbf{Q}$   
 $\mathbf{Q}^{-1}$  = inverse matrix of  $\mathbf{Q}$

### 3.2 Proposed weighted coherence estimator

As an unknown parameter, the coherence magnitude  $\gamma$  can be estimated by maximizing (5) or, equivalently, the log of (5), based on the ML principle. The log of (5) is easily gotten as:

$$\ln p(\mathbf{X} | \gamma, \varphi) = -2N \ln \pi - N \ln |\mathbf{Q}| - \sum_{k=1}^N \mathbf{X}_k^H \mathbf{Q}^{-1} \mathbf{X}_k. \quad (6)$$

In the rest of this paper, the summation symbol  $\sum_{k=1}^N$  is replaced with  $\sum$  to simply the notation. Then taking the partial derivative of (6) with respect to  $\gamma$  and setting the result to zero gives:

$$-\frac{N}{|\mathbf{Q}|} \frac{\partial(|\mathbf{Q}|)}{\partial \gamma} - \sum \mathbf{X}_k^H \frac{\partial(\mathbf{Q}^{-1})}{\partial \gamma} \mathbf{X}_k = 0. \quad (7)$$

Here,  $|\mathbf{Q}|$  and  $\mathbf{Q}^{-1}$  can be easily gotten according to the definition of the covariance matrix  $\mathbf{Q}$ . Then we can obtain the following partial derivations after a number of algebraic manipulation:

$$\begin{aligned} \frac{\partial |\mathbf{Q}|}{\partial \gamma} &= -2\gamma \sigma_f^2 \sigma_g^2; \\ \frac{\partial(\mathbf{Q}^{-1})}{\partial \gamma} &= \frac{2\gamma}{(1-\gamma^2)^2} \begin{bmatrix} \frac{1}{\sigma_f^2} & -\frac{\gamma e^{j\varphi}}{\sigma_f \sigma_g} \\ -\frac{\gamma e^{-j\varphi}}{\sigma_f \sigma_g} & \frac{1}{\sigma_g^2} \end{bmatrix} \\ &+ \frac{1}{1-\gamma^2} \begin{bmatrix} 0 & -\frac{e^{j\varphi}}{\sigma_f \sigma_g} \\ -\frac{e^{-j\varphi}}{\sigma_f \sigma_g} & 0 \end{bmatrix}. \end{aligned} \quad (8)$$

Substituting  $|\mathbf{Q}|$ ,  $\mathbf{Q}^{-1}$ , and (8) into (7) and setting the result to zero, we have:

$$\frac{2N\gamma}{1-\gamma^2} - \frac{1}{(1-\gamma^2)^2} \left[ 2\gamma \left( \frac{\sum f_k^* f_k}{\sigma_f^2} + \frac{\sum g_k^* g_k}{\sigma_g^2} \right) \right] = 0. \quad (9)$$

Substituting the following reasonable approximations:

$$\sigma_f^2 \approx \frac{1}{N} \sum f_k^* f_k; \sigma_g^2 \approx \frac{1}{N} \sum g_k^* g_k, \quad (10)$$

into (9), then dividing through by  $1+\gamma^2$  and simplifying, we can obtain:

$$\gamma = \frac{e^{-j\varphi} \sum f_k g_k^* + e^{j\varphi} \sum f_k^* g_k}{\frac{\sigma_g}{\sigma_f} \sum f_k^* f_k + \frac{\sigma_f}{\sigma_g} \sum g_k^* g_k}. \quad (11)$$

Using the ML estimate of the phase difference  $\varphi$  (Rodríguez, Martín, 1992), we get the following relationship:

$$e^{j\hat{\varphi}_k} \sum f_k^* g_k = e^{-j\hat{\varphi}_k} \sum f_k g_k^* = \left| \sum f_k^* g_k \right|. \quad (12)$$

Substituting (12) into (11) and setting the ratio of the true variance as  $R = \sigma_f^2 / \sigma_g^2$ , we have:

$$\hat{\gamma} = \frac{2 \left| \sum f_k^* g_k \right|}{\sum f_k^* f_k / \sqrt{R} + \sqrt{R} \sum g_k^* g_k}. \quad (13)$$

The coherence metric  $\hat{\gamma}$  can be viewed as a weighted form of the estimator  $\hat{\gamma}_m$ . A comparison between  $\hat{\gamma}$  and the above-mentioned estimators  $\hat{\gamma}_c$  and  $\hat{\gamma}_m$  is firstly performed below. According to the inequality properties, we can easily get the following relationship:

$$\sum f_k^* f_k / \sqrt{R} + \sqrt{R} \sum g_k^* g_k \geq 2\sqrt{\sum f_k^* f_k \sum g_k^* g_k}. \quad (14)$$

Therefore,  $\hat{\gamma}$  is less than or equal to  $\hat{\gamma}_c$ . Combing the definition of  $R$  and (10), we can obtain:

$$\sum f_k^* f_k \approx R \sum g_k^* g_k. \quad (15)$$

Then the difference  $\Delta$  of the denominators of estimators  $\hat{\gamma}$  and  $\hat{\gamma}_m$  can be expressed as:

$$\begin{aligned} \Delta &= \sum f_k^* f_k / \sqrt{R} + \sqrt{R} \sum g_k^* g_k - (\sum f_k^* f_k + \sum g_k^* g_k) \\ &\approx (\sqrt{R} - 1)^2 \sum g_k^* g_k. \end{aligned} \quad (16)$$

Thus,  $\hat{\gamma}$  is more than or equal to  $\hat{\gamma}_m$ . Consequently,  $\hat{\gamma}$  seems more likely a compromise between estimators  $\hat{\gamma}_c$  and  $\hat{\gamma}_m$ , indicating the introduction of the weights in  $\hat{\gamma}$  can improve the values of  $\hat{\gamma}_m$  to some extent. However, in CCD, we expect to lower the coherence magnitude in change regions to improve the contrast between the changed areas and the background (unchanged areas). Inspired by the idea, the new weighted estimator is defined as

$$\hat{\gamma}_w = \frac{2 \left| \sum_{k=1}^N f_k^* g_k \right|}{\sqrt{R} \sum_{k=1}^N f_k^* f_k + \sum_{k=1}^N g_k^* g_k / \sqrt{R}}. \quad (17)$$

Notice that the weights of  $\hat{\gamma}_w$  are replaced with the reciprocals of that of  $\hat{\gamma}$  to decrease the coherence in change areas. The rationality of the definition will be experimentally demonstrated on simulated SAR images in Section 4.

## 4. EXPERIMENTAL RESULTS

In order to assess the effectiveness of the proposed estimator, we first performed a simulation with known true-variance ratios to compare the change detection performance of  $\hat{\gamma}_c$ ,  $\hat{\gamma}_m$ , and the proposed  $\hat{\gamma}_w$ . Then we compared the detection performance of  $\hat{\gamma}_w$  with the other three estimators  $\hat{\gamma}_c$ ,  $\hat{\gamma}_m$ , and  $\hat{\gamma}_a$  on the real SAR images. Furthermore, a brief comparison between  $\hat{\gamma}_m$ , the mean-ratio operator, and  $\hat{\gamma}_w$  was performed to illustrate the advantages of the introduction of weights.

#### 4.1 Simulated Data Example

To verify the theoretical feasibility of the method, we simulated a SAR image pair with a size of  $2000 \times 2000$ . In the simulation process, we adopt the hypothesis tests as (Cha et al., 2015):

$$\begin{aligned} H_0^{1st} : \sigma_f &\approx \sigma_g & H_1^{1st} : \sigma_f &\neq \sigma_g \\ H_0^{2nd} : \gamma &\approx 1 & H_1^{2nd} : \gamma &< 1. \end{aligned} \quad (18)$$

According to the tests, there are four possible combination cases:  $H_0^{1st} + H_0^{2nd}$ ,  $H_0^{1st} + H_1^{2nd}$ ,  $H_1^{1st} + H_0^{2nd}$ , and  $H_1^{1st} + H_1^{2nd}$ . Similarly, we also accept  $H_1^{1st} + H_0^{2nd}$  is unlikely to happen. Therefore, only the other three cases are considered in the simulation. One point to be mentioned here is that the simulation depends on the real and imaginary components of the SAR complex image are the independent identically distributed zero-mean Gaussian random variables.

Under hypothesis test  $H_0^{1st} + H_0^{2nd}$ , SAR images are simulated with similar intensities and high coherence values, indicating that no changes have occurred between the simulated images. For this purpose, two components of one complex SAR image are firstly randomly simulated, then the other image is simulated by adding a Gaussian noise for two components, respectively.

In the condition of  $H_0^{1st} + H_1^{2nd}$  and  $H_1^{1st} + H_1^{2nd}$ , the simulated SAR images have low coherence values. The corresponding SAR image pairs of the two cases are thus generated using a random Gaussian complex simulation to keep the low-coherence property. Test combination  $H_1^{1st} + H_1^{2nd}$  happens mainly in vegetation or low-CNR areas. For two repeat-pass SAR images, although decorrelation, there is unlikely to exist significant intensity differences in these areas where no features have changed. Differently, low coherence and obvious intensity differences generally indicate a true temporal change has occurred between two SAR images. This situation is in accord with  $H_1^{1st} + H_1^{2nd}$ . Therefore, we would expect the coherence estimator to be able to distinguish the two cases, identifying change regions from low-coherence regions instead of just highlighting all low-coherence areas.

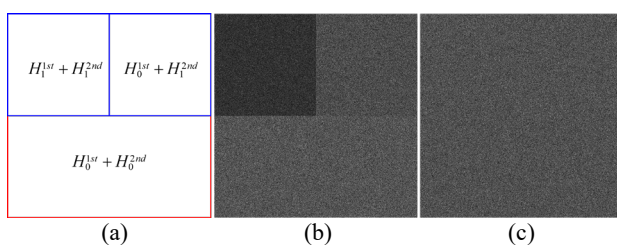


**Figure 1.** The simulation frame and the real components of the simulated SAR image pair.

To better demonstrate the effect of the estimator, the simulated SAR image is divided into three parts: the upper-left block of the size of  $1000 \times 1000$  based on  $H_1^{1st} + H_1^{2nd}$ , the upper-right block of the size of  $1000 \times 1000$  based on  $H_0^{1st} + H_1^{2nd}$ , and the lower block of the size of  $1000 \times 2000$  based on  $H_0^{1st} + H_0^{2nd}$  (see the simulation frame shown in Figure 1 (a)). Since adopting the same simulation way of two components, here we just give the real components of the simulated image pair as shown in Figure 1(b) and (c). Note that the upper two blocks correspond to low-coherence areas, and the lower block to the high-coherence area.

In this experiment, the true variance of the second image  $\sigma_g^2$  is assumed to 1.0. The ratio  $R$  is set to 0.5 and 0.9 for the upper-left and upper-right blocks, respectively. For the lower block, the variance of the additive noise is set to half of  $\sigma_g^2$ .

Practically, raw estimator outputs are often called SAR change detection images in CCD (Cha et al., 2015). Figure 2 shows SAR change detection images of the simulated images estimated using  $\hat{\gamma}_c$ ,  $\hat{\gamma}_m$ , and the proposed  $\hat{\gamma}_w$ , respectively. The following conclusions can be drawn.

- 1) In low-coherence areas, all estimators can get low coherence values. However, the detection image estimated by  $\hat{\gamma}_c$  has no obvious difference between blocks with different  $R$  values, which means that  $\hat{\gamma}_c$  fails to identify change areas from all decorrelation areas. The estimator  $\hat{\gamma}_m$  is comparatively better than  $\hat{\gamma}_c$ , keeping consistent with the conclusion proved by Cha et al.. Note that the proposed  $\hat{\gamma}_w$  yield the higher-contrast detection image among three estimators. In the simulated image block based on  $H_0^{1st} + H_1^{2nd}$ , the detection results obtained by the three estimators are visually similar in brightness but significantly different in the block based on  $H_1^{1st} + H_1^{2nd}$ . The proposed estimator can provide much lower coherence values than  $\hat{\gamma}_c$  and  $\hat{\gamma}_m$  in the block with obvious intensity differences and low coherence, making the boundary between the two types of decorrelation areas much clearer. Since the two blocks in the low-coherence case are simulated in the same way, the only difference is the true variance ratio used. Therefore, the proposed coherence estimator  $\hat{\gamma}_w$  is also sensitive to the ratio  $R$  and more effective for highlighting changes.
- 2) In high-coherence areas, all estimators can provide high coherence values, making the detection image blocks fill with bright pixels. And there are no obvious differences between the detection results of the three estimators.

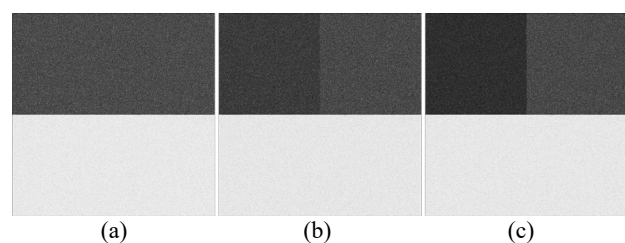


**Figure 2.** SAR change detection images of the simulated SAR image pairs using different coherence estimators. (a)  $\hat{\gamma}_c$ . (b)  $\hat{\gamma}_m$ . (c) Proposed  $\hat{\gamma}_w$ .

To sum up, the new estimator can give the best performance among the three estimators in theory: the contrast between low- and high-coherence areas is most obvious and the two types of low-coherence regions can be effectively distinguished. As we know, CCD aims at detecting changes that have occurred between two SAR images, therefore, an optimal coherence estimator should provide a change detection image where the contrast of the change areas and the background (unchanged areas) should be as obvious as possible, restraining the information of the background and enhancing the change information to the greatest extent (Gong et al., 2012). Therefore, our weighted estimator is comparatively more suitable for CCD tasks.

## 4.2 Real Data Example

The weighted estimator was also used on a section (1000×1000 pixels) of the real SAR image pair taken by the TerraSAR-X satellite in an area with various features, such as buildings, water, and mountains, in February and May 2013, respectively. Between the two data acquisitions, the ice in water areas melts as the weather warms up. Therefore, this image pair is selected for detecting ice-change areas. The available ground truth (reference image) shown in Figure 3(c) was determined by visual inspection based on the input images in Figures 3(a) and (b). In this experiment, the proposed  $\hat{\gamma}_w$  is compared with the other three coherence estimators:  $\hat{\gamma}_c$ ,  $\hat{\gamma}_m$ , and the CRCD metric that will be referred to as  $\hat{\gamma}_\alpha$  for ease of comparison.

For all methods, the window size to estimate the coherence values for each pixel is set to 3×3. Since the additive noise is regarded as constant throughout the scene, it can be measured in regions with low average backscatter coefficient (Carrara, Goodman, and Majewski, 1995). Here, the additive noise values required by estimator  $\hat{\gamma}_\alpha$  are measured in a manually selected shadow area following the process introduced by Wahl (2016). As the proposed  $\hat{\gamma}_w$  needs the ratio  $R$  corresponding to each pixel in the SAR image, the window size for estimating  $R$  is set to 3×3 to reduce the influence of speckles.

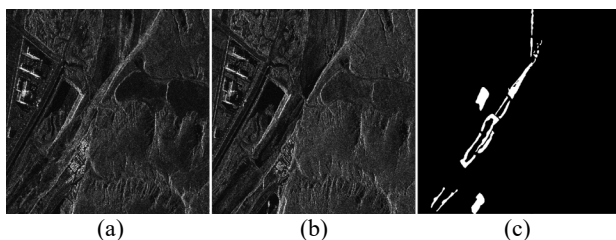


**Figure 3.** Multitemporal SAR image pair used in the experiment. (a) Image acquired in February 2013 covering frozen water areas. (b) Image acquired in May 2013 covering unfrozen water areas. (c) Ground truth.

Figure 4 illustrates SAR change detection images of  $\hat{\gamma}_c$ ,  $\hat{\gamma}_m$ ,  $\hat{\gamma}_\alpha$ , and the proposed  $\hat{\gamma}_w$ , respectively, prior to thresholding. Notice that the coherence values of most areas are very low except for some building areas in the detection images. One point to be mentioned here that some low-CNR areas in the detection image of  $\hat{\gamma}_\alpha$ , such as roads and shadow areas, are filled with bright pixels with high coherence values due to the introduction of the additive thermal noise. In Figure 4(a), all decorrelation regions caused by different sources exhibit similar characteristics in brightness, indicating the failure of  $\hat{\gamma}_c$  in detecting changes. The image in Figure 4(b) with  $\hat{\gamma}_m$  differentiates the ice-change areas, filling them with darker pixels. Meanwhile, we found that  $\hat{\gamma}_\alpha$  gives a similar detection result as  $\hat{\gamma}_m$  except for some low-CNR areas. Although the two estimators have achieved some performance, the boundaries between the changed and unchanged areas in detection images are not particularly clear, which can be further demonstrated by the close-up images in Figures 5(b) and (c). By contrast, the image in Figure 4(d) with the novel estimator significantly improves the result from  $\hat{\gamma}_m$  by effectively emphasizing the changes, presenting the highest contrast among the four estimators.

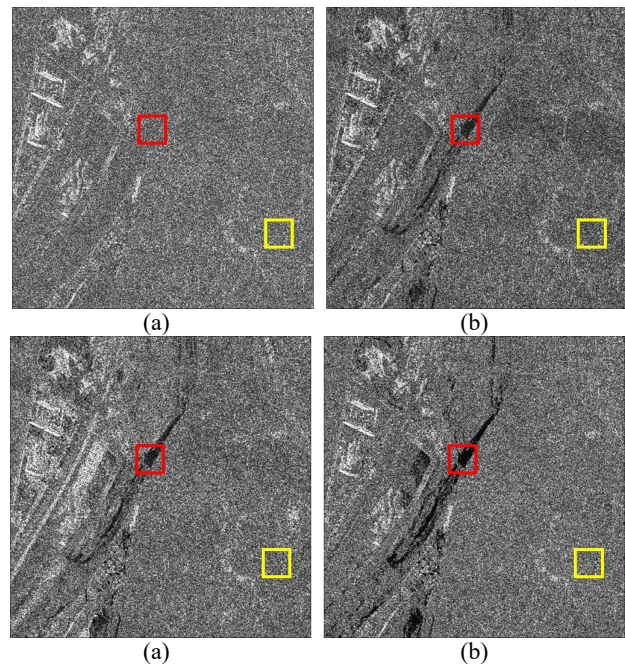


**Figure 4.** SAR change detection images of the real SAR image pair estimated using different estimators. (a)  $\hat{\gamma}_c$ . (b)  $\hat{\gamma}_m$ . (c)  $\hat{\gamma}_\alpha$ . (d) Proposed  $\hat{\gamma}_w$ .

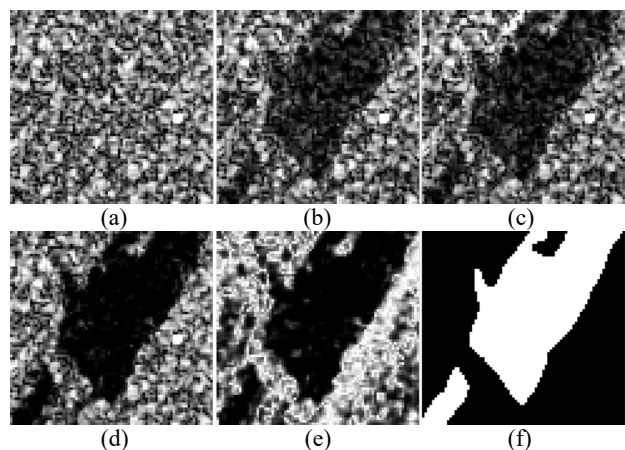


**Figure 5.** The close-up view of the red rectangle in Figure 4 with (a)  $\hat{\gamma}_c$ , (b)  $\hat{\gamma}_m$ , (c)  $\hat{\gamma}_\alpha$ , and (d) Proposed  $\hat{\gamma}_w$ , (e) the mean-ratio operator, and (f) corresponding ground truth.

Smaller portions corresponding to the red rectangle in Figure 4 are shown in Figure 5(a)-(d) to further demonstrate the difference between the four methods in ice-change regions. Figure 5(f) is the corresponding ground truth in this area. Notice that the detection result of  $\hat{\gamma}_c$  mixes the change areas with other decorrelation areas, failing to identify changes. Although having similar detection results,  $\hat{\gamma}_\alpha$  performs slightly better than  $\hat{\gamma}_m$  by filling the ice-change areas with darker pixels. However, it can be seen that the boundaries between the changed and unchanged regions are very unclear, making it difficult to get the high-precision detection result. Compared with  $\hat{\gamma}_m$  and  $\hat{\gamma}_\alpha$ , we observe from Figure 5(d) a significant contrast enhancement using  $\hat{\gamma}_w$ , providing much lower coherence values in change

areas. Therefore, the proposed  $\hat{\gamma}_w$  is more effective than the other estimators in highlighting changes.

Since  $\hat{\gamma}_w$  can be seen as a weighted form of  $\hat{\gamma}_m$  by introducing the corresponding parameters about the ratio change statistic of noncoherent intensity-based methods, we also validate the robustness of our method by comparison with  $\hat{\gamma}_m$  and the mean-ratio operator. Two points need to be noted here: one is the difference image obtained using the change statistic in intensity-based methods is also referred to as SAR change detection image for consistency; the other is the mean-ratio operator used in this paper, different from the commonly used one (Inglada, Mercier, 2007), does not need to be subtracted by 1.0, making the change areas of its detection result fill with dark pixels as the same as the coherence estimators.

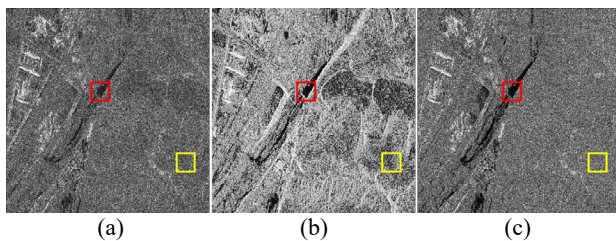


**Figure 6.** SAR change detection results using different change statistics. (a)  $\hat{\gamma}_c$ . (b) Mean-ratio operator in noncoherent intensity-based methods. (c) Proposed  $\hat{\gamma}_w$ .

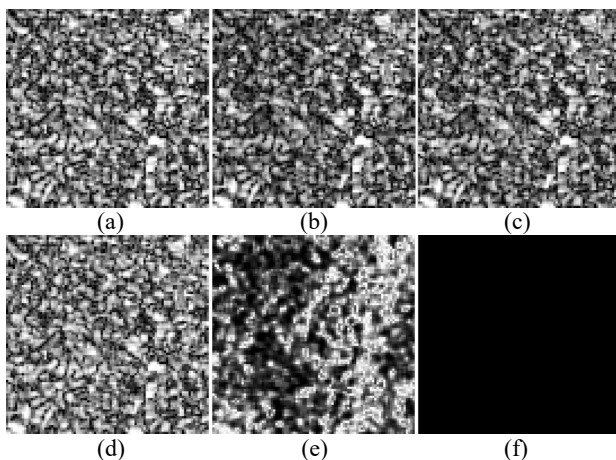


**Figure 7.** The close-up view of the yellow rectangle in Figure 4 with (a)  $\hat{\gamma}_c$ , (b)  $\hat{\gamma}_m$ , (c)  $\hat{\gamma}_\alpha$ , and (d) Proposed  $\hat{\gamma}_w$ , (e) the mean-ratio operator, and (f) corresponding ground truth.

Figure 6 shows the raw outputs of  $\hat{\gamma}_m$ , the mean-ratio operator, and  $\hat{\gamma}_w$ , respectively. As an intensity-based method, the mean-ratio operator is sensitive to the difference in intensity, providing low values in ice-changed areas. However, it is the sensitivity that leads to low values in regions of weak changes that can be caused by vegetation growth and other reasons. The close-up views of the red and yellow rectangles in Figure 4 are shown in Figures 5 and 7, respectively, to further illustrate the effectiveness of the new estimator. It is observed from Figure 5(e) that the mean-ratio operator can provide low values in change areas of significant intensity difference and yield a high-contrast detection image. However, in weak-change regions, as circled by the yellow rectangle, this operator can still provide low values (see Figure 7(e)). The coherent detection results in

Figure 7(a)-(d) and the result of manual visual interpretation in Figure 7(f) show that no changes have occurred between the two collections in this region. These low-value areas estimated by the mean-ratio operator thus would bring trouble in obtaining final detection results. By comparison, the novel estimator  $\hat{\gamma}_w$  combines the advantages of the mean-operator and the coherent estimators, displaying a clear boundary of the change area and not so sensitive to intensity differences in weak-change regions (see Figure 5(d) and Figure 7(d)). It can be concluded that the introduction of the ratio change statistic into the coherence estimator enables the new statistic to largely combine the advantage of the two types of change detection algorithms.

## 5. CONCLUSION

In this paper, we have derived a new weighted coherence estimator for SAR CCD based on the statistical properties of SAR images and the ML principle. The estimator has been shown to have a better change detection performance over the current classic estimators by effectively highlighting the changes. The significant improvement in detection performance was achieved due to the introduction of the weights of the ratio change statistic, combining the advantages of the coherent and noncoherent change detection algorithms. Furthermore, the introduction of weights also makes the estimator no longer need to satisfy the equal-variance assumption. The proposed coherence estimator was calculated for both simulated and real SAR images, experimentally demonstrating its effectiveness and feasibility.

## REFERENCES

- Carrara, W. G., Goodman, R. S., Majewski, R. M., 1995: *Spotlight Synthetic Aperture Radar: Signal Processing Algorithms*. Artech House, Boston.
- Cha, M., Phillip, R. D., Wolfe, P. J., Richmond, C. D., 2015. Two-stage change detection for synthetic aperture radar. *IEEE Trans. Geosci. Remote Sens.*, 53(12), 6547-6560.
- Gong M., Zhou Z., Ma J., 2012. Change Detection in Synthetic Aperture Radar Images Based on Image Fusion and Fuzzy Clustering. *IEEE Trans. Imag. Process.*, 21(4), 2141-2151.
- Guarnieri, A. M., Prati, C., 1997: SAR Interferometry: A “Quick and Dirty” Coherence Estimator for Data Browsing. *IEEE Trans. Geosci. Remote Sens.*, 35, 660-669.
- Hanssen, R. F., 2001: *Radar Interferometry: Data Interpretation and Error Analysis*. Kluwer Academic publishers, Dordrecht.
- Inglada, J., Mercier, G., 2007. A New Statistical Similarity Measure for Change Detection in Multitemporal SAR Images and Its Extension to Multiscale Change Analysis. *IEEE Trans. Geosci. Remote Sens.*, 45(5): 1432-1445.
- Jakowatz, C. V., Jr., Wahl, D. E., Eichel, P. H., Ghiglia, D. C., Thompson, P. A., 1996: *Spotlight-mode Synthetic Aperture Radar: A Signal Processing Approach*. Kluwer Academic publishers, Boston.
- Massonnet, D., Feigl, K. L., 1998. Radar Interferometry and Its Application to Changes in the Earth’s Surface. *Rev. Geophys.*, 36(4), 441-500.

Oliver C., Quegan, S., 2004. *Understand. Synthetic Aperture Radar Images*. SciTech Publishing, Raleigh.

Preiss, M. A., Gray, D. A., Stacy, N. J. S., 2006. Detecting Scene Changes Using Synthetic Aperture Radar Interferometry. *IEEE Trans. Geosci. Remote Sens.*, 44(8), 2041-2054.

Rodriguez, E., Martin, J. M., 1992. Theory and Design of Interferometric Synthetic Aperture RADARS. *Proc. Inst. Elect. Eng.—F Radar Signal Process.*, 139(2), 147-159.

Wahl, D. E., Yocky, D. A., Jakowatz, C. V., Simonson, K. M., 2016. A New Maximum-Likelihood Change Estimator for Two-Pass SAR Coherent Change Detection. *IEEE Trans. Geosci. Remote Sens.*, 54(4), 2460-2469.

Yang X., Xu D., Huang P., Yang W., 2015. Change Detection of High Resolution SAR Images by the Fusion of Coherent/Incoherent Information. *J. Radars*, 4(5), 582-590.

Yocky, D. A., Johnson, B. F., 1998. Repeat-Pass Dual-Antenna Synthetic Aperture Radar Interferometric Change Detection Post Processing. *Photogramm. Eng. Remote Sens.*, 64(5), 425-429.

Zhao J., Liang X., Li Y., 2017. Change Detection in SAR CCD Based on the Likelihood Change Statistics. *J. Radars*, 6(2), 186-194.